ACS OMEGA

Open Access

http://pubs.acs.org/journal/acsodf

Article

Preparation and Characterization of Ultrafine Nitroguanidine with Different Aspect Ratios

Dan Liang, Wenjing Zhang, Xiaoan Wei,* Sheng Wang, Binbin Wang, and Zeshan Wang

Cite This: *ACS Omega* 2024, 9, 538−544

Read Online

ACCESS | Metrics & More | Article Recommendations

ABSTRACT: In order to improve the mechanical properties and thermodynamic stability of the long needle-like raw material Nitroguanidine (NQ), it was pulverized by a mechanical pulverization method and dried by a spray drying method, and three ultrafine NQ samples with different aspect ratios (2.26, 1.87, and 1.25) were prepared. The samples were tested and characterized by scanning electron microscopy, digital imaging particle size analysis, X-ray diffraction, and differential scanning calorimetry (DSC), and the impact sensitivity and bulk density of the raw NQ and ultrafine NQ samples were also tested. The results show that ultrafine NQ has the smallest particle size D_{50} of 9.18 μm, with uniform particle size distribution, unchanged crystal structure, and no introduction of impurities, and the impact sensitivity was the same as that of the feedstock NQ, which was 0. In addition, with the decreasing aspect ratio of the NQ particles, their apparent activation energy increased, and the energy required to be absorbed in the thermal decomposition increased; their thermal stability was also better.

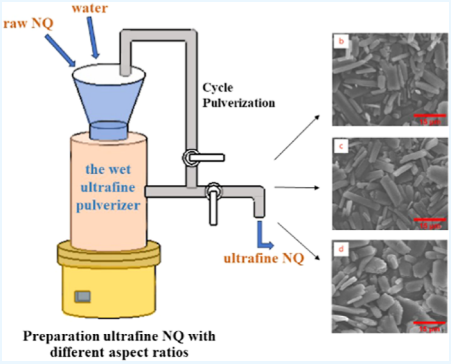

1. INTRODUCTION

Nitroguanidine (NQ) is a low-vulnerability explosive with good explosive properties and stability and is commonly used as an important component of launching charges and propellants.[1−3] Raw material NQ is a kind of long needlelike crystal with a large aspect ratio, which inevitably causes stress concentration at the tip, and its disadvantages of crystal defects and poor dispersion adversely affect the mechanical properties and combustion properties of the charge. Destroying its needle-like structure, eliminating stress concentration at its tip, and improving its dispersion properties are the keys to solving this problem.[4,5]

The crystal morphology and particle size of explosives directly affect the physicochemical properties of explosives. A large number of studies have shown that, ultrafine explosives, due to the reduction of particle size and increase in specific surface area, have the advantages of more complete energy release, more stable propagation of the explosion wave, and lower explosibility.[6,7] Even for ultrafine explosives with a particle size of about 10 μm, their physicochemical properties are very different.[8]

In recent years, the main ways to improve the mechanical properties and thermodynamic stability of NQ have been through physical and chemical methods, with ultrasonic pulverization, grinding refinement, and impact crushing refinement as the main physical methods and solvent−nonsolvent recrystallization refinement and microemulsification refinement as the main chemical methods.[9−12] The use of physical methods for pulverization suffers from the shortcomings of safety, energy consumption, and the difficulty of controlling the crystal size distribution and the regularity of the crystal shape. The recrystallization of NQ by chemical methods increases the unsafe factor due to the volatility and combustion of organic solvents such as DMF, NMP, and acetone, as well as the consumption and recycling costs of solvents and new sources of pollution. Therefore, it is of practical significance to study the preparation method of ultrafine NQ that can effectively improve the crystal morphology and particle size of NQ, and the preparation process meets the requirements of safety and green chemistry.

In this study, the raw material NQ was pulverized by a mechanical method and dried by a spray drying method, and ultrafine NQ with a shorter aspect ratio and better dispersion compared with the raw material was successfully prepared by controlling the process conditions. In this method, during the pulverization process, the raw material NQ was directly put into water, and the water was used as a stabilizing agent without adding any organic solvent, and the long needle-like raw material NQ is directly pulverized by the ultrahigh-speed shear effect of the wet ultrafine pulverizer. In addition, using the spray drying method for drying, hot air and spray material liquid contact, and

Received: August 17, 2023
Revised: November 24, 2023
Accepted: November 28, 2023
Published: December 19, 2023

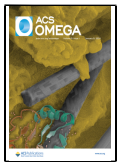

https://doi.org/10.1021/acsomega.3c06086
ACS Omega 2024, 9, 538−544

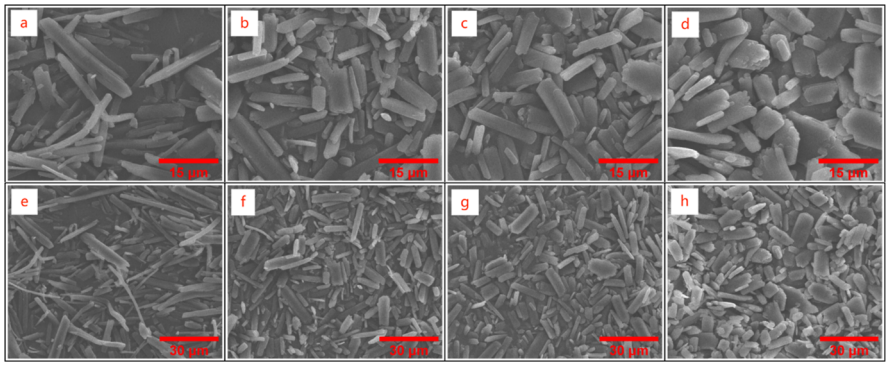

Figure 1. SEM images of raw NQ (a, e), ultrafine NQ 1# (b, f), ultrafine NQ 2# (c, g), and ultrafine NQ 3# (d) (h).

the temperature is rapidly reduced. Therefore, controlling the hot air in a certain temperature range can ensure a higher drying efficiency and also avoid the drying of materials subjected to excessive heat, leading to thermal decomposition brought about by safety issues.

2. MATERIALS AND METHODS

2.1. Materials and Instruments. Materials: raw material NQ, chemically pure, manufactured in Shanxi Jianghuai Heavy Industry Co., Ltd., China.

Instruments: S-3400N scanning electron microscope (SEM), Hitachi, Japan; Camsizer X2 Digital Imaging Particle Size Analyzer, Microtrac Retesh, Germany; D8 ADVANCE X-ray diffractometer, Bruker, Germany; and DSC 204 F1 Phoenix differential scanning calorimeter, Netzsch, Germany.

2.2. Methods. Nitroguanidine is put into water in a certain proportion (the mass ratio of NQ to water is 1:9), a small amount of surfactant is added, and the suspension slurry is stirred thoroughly. The slurry is continuously fed into the grinding chamber of the wet ultrafine pulverizer using a circulating pump, and the speed of the working head of the instrument is set to 6000 rpm through the friction and shear force between the ultrahigh-speed rotating disk mill and fixed disk mill of the equipment. It makes full use of shearing, grinding, high-speed mixing, and other roles to break up and disperse the long-needle NQ in the raw material liquid. The NQ internal defects at the formation of stress concentration are first fractured, the particle aspect ratio decreases, and small particles are formed. Then, through the material cycle, small particles in the uniform crushing force field of repeated action ultimately become a larger degree of sphericality, and obtain ultrafine granular NQ with fewer crystal defects. The number of pulverizing cycles was recorded, and the number of crushing cycles of 3 times, 4 times, and 5 times of the material liquid samples, respectively, were numbered as 1 #, 2 #, and 3 #.

The refined NQ material liquid is discharged to the storage tank through a 5 μm screen, the material liquid is continuously input to the high-speed centrifugal spray dryer by a diaphragm pump, the atomizer nozzle sprays out the mist droplets, and then it drops with hot air in parallel flow, and the temperature of the hot air is controlled to be below 60 °C. The surface area of the material liquid is greatly increased after atomization, and the rapid evaporation of water can be realized in the air flow. The surface area of the material liquid is greatly increased after atomization, the rapid evaporation of water can be realized in the airflow, and the ultrafine NQ obtained by drying at the bottom of the tower has uniform particle size, good dispersion, and there is no agglomeration of particles.

2.3. Characterization. The particle morphology and size of the samples were observed using a scanning electron microscope; the samples were sprayed with gold under vacuum conditions; and the accelerating voltage for the test was 15.0 kV.

The particle size distribution of samples is examined using the Camsizer X2 digital imaging particle size analyzer.[13] In the particle size test, the X-Jet module is used. The sample enters the test chamber through dry powder feeding and pressurized dispersion (250 kPa) and is captured by the CCD lens in real time. The reference lens (B-CCD) records the particle size and morphology of the large particles, and the focusing lens (Z-CCD) records the particle size and morphology of the small particles.

The sample crystallites were characterized using an X-ray diffractometer with a scanning step of 0.05° and a scanning angle of 2θ ranging from 10 to 50°.

The impact sensitivity was determined by the drop hammer method,[14] with reference to the Chinese military standard (GJB 772A-97 method), and a drop hammer mass of 10 kg was selected with a drop height of 50 cm and a sample mass of 50 ± 1 mg, and 25 rounds of each specimen were tested to make two sets of parallel experiments. The standard container method was used to measure the bulk density of the samples. At a certain temperature, the specimen from the funnel free fell and was filled with a volume of 20 mL of standard containers, with a scraper vertically in contact with the upper edge of the standard containers and one-way uniform scraping across the surface, gently tapping the standard containers filled with specimens, and standard containers of the outer surface of the powder wiped away. The ratio of the mass of the specimen in the standard cup to the volume it occupies is the bulk density of the specimen.

Differential scanning calorimetry (DSC) was used to determine the decomposition temperature of the samples at 5, 10, 15, and 20 K/min heating rates. The samples were heated in a crimped aluminum crucible under a nitrogen atmosphere at a flow rate of 40 mL/min for 0.7 ± 0.2 mg samples, and the test temperatures ranged from 220 to 300 °C.

3. RESULTS AND DISCUSSION

3.1. Particle Morphology Characterization. Figure 1 shows SEM images of the raw NQ and ultrafine NQ samples. From Figure 1a,e, the raw material NQ consists of long needle-like crystals, the particle length is about 30−50 μm, the stress at the tip is concentrated, there are crystal defects, the particles are intertwined with each other, and the dispersion is poor. From Figure 1b,F, for ultrafine NQ (1#) samples, after three times of pulverization, the particle size of the particles was in in teens of microns; from Figure 1c,g, for ultrafine NQ (2#) samples, after

https://doi.org/10.1021/acsomega.3c06086
ACS Omega 2024, 9, 538−544

four times of pulverization, the particle size compared to the 2# samples has been reduced, and the shape of the shape of the rectangular; and from Figure 1d,h, for ultrafine NQ (3#) samples, after five times of pulverization, the sample particles have a diameter of about 10 μm square-like. The test results show that the NQ particles are first destroyed at the stress concentration when crushed; with the increase of the number of crushing cycles, the width of the particles does not change significantly, but the long-needle structure is broken, the particle aspect ratio decreases, the particles change from long-needle to rectangular and then gradually change to square-like, the crystal defects are modified, and the dispersion is improved.

3.2. Particle Size Distribution. From the SEM images, it can be seen that the width of the ultrafine NQ particles did not change significantly, and the aspect ratio decreased continuously with the increase in the number of pulverization cycles. Therefore, the test method of using the diameter of spherical particles as the equivalent particle size to represent the diameter of nonspherical particles in the particle size testing by laser particle size instruments is not applicable to the particle size testing of NQ particles after pulverization by this mechanical method.[15]

The particle size distribution of raw NQ and ultrafine NQ samples was characterized using the Camsizer X2 digital imaging particle size analyzer, and the results are shown in Table 1.

Table 1. Particle Size Distribution of Raw NQ and Ultrafine NQ Samples

sample	pulverization (times)	particle size (μm)			average aspect ratio
		D_{10}	D_{50}	D_{90}	
raw NQ	0	21.52	38.44	63.78	8.73
1#	3	7.28	12.54	18.79	2.26
2#	4	7.08	10.28	16.01	1.83
3#	6	5.78	9.18	13.08	1.25

Figure 2 shows the particle size distribution of the raw NQ and ultrafine NQ samples, and the horizontal coordinate X_{Fe_max} is the maximum Feret diameter, which indicates the particle size defined in terms of particle length; the vertical coordinate Q_3 is the cumulative volume percentage, which refers to the ratio of the volume of the particles with a particle size less than X_{Fe_max} to the total volume; and q_3 is the bulk density profile, which refers to the ratio of the volume of particles per unit size particle to the total volume.[13]

As can be seen from Figure 2a, the particle size distribution of the raw NQ is wide, ranging from a dozen micrometers to hundreds of micrometers, and the particle size distribution is not uniform. From Table 1 and Figure 2b, it can be seen that the D_{50} of the ultrafine NQ samples (1#, 2#, and 3#) are 12.36, 10.98, and 9.43 μm, respectively, and the particle size distribution is within 25 μm. In addition, the 3# sample with ultrafine NQ has the most concentrated particle size distribution, more uniform particle size, and the best effect of ultrafine. This indicates that with the increase of the number of cycle pulverization, the particle size of NQ particles keeps getting smaller, and the particle size distribution is more uniform.

Figure 3 shows the width-to-length ratio curves of raw NQ and ultrafine NQ samples, from which it can be seen that the raw NQ has a smaller width-to-length ratio, that is, a larger aspect ratio, while the ultrafine NQ sample has a smaller length-to-diameter ratio. Therefore, the stress concentration and crystal

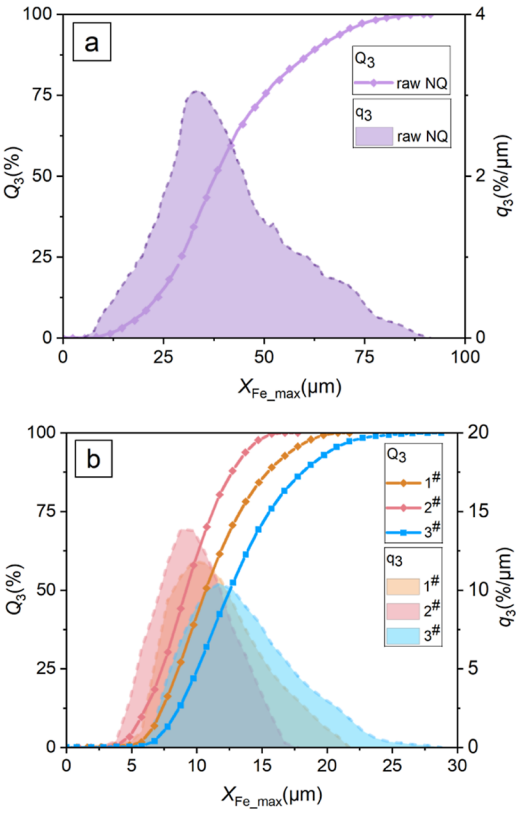

Figure 2. Cumulative particle size distribution of raw NQ (a) and ultrafine NQ 1# 2# 3# sample (b).

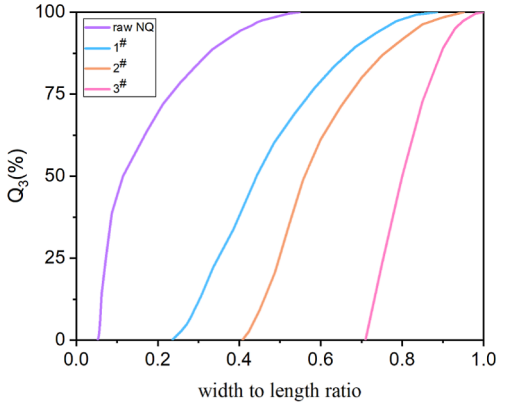

Figure 3. Aspect width-to-length ratio curves of raw NQ and ultrafine NQ samples.

defects of the original NQ brought on by the long needle structure are modified.

3.3. Crystal Structure Analysis. X-ray diffraction (XRD) analysis of the raw NQ and ultrafine NQ samples was carried out to examine whether the crystal structure of the raw NQ changed after pulverization, and the results are shown in Figure 4. As can be seen from Figure 4, the diffraction peaks of the ultrafine NQ samples maintained the same position as those of the raw material NQ,[16] indicating that the crystal structure of the ultrafine NQ samples did not change and no impurities were introduced during the mechanical pulverization process.

From Figure 4, it can also be seen that the intensity of the peaks of the ultrafine NQ samples is different from that of the raw NQ, and the diffraction peaks around 17.4° are significantly

https://doi.org/10.1021/acsomega.3c06086
ACS Omega 2024, 9, 538−544

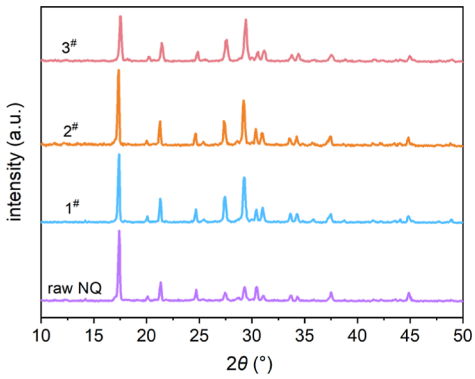

Figure 4. XRD patterns of raw NQ and ultrafine NQ samples.

shorter, which may be due to the change in the crystal structure after pulverization of the NQ particles and the damage to the crystal surface.[17] In addition, the XRD diffraction peaks of the ultrafine NQ samples were broadened relative to those of the raw NQ. According to the Scherrer equation, the particle size is inversely proportional to the half-peak width of its diffraction peaks, and it is the reduction of the particle size of ultrafine NQ that leads to the broadening of its diffraction peaks.

3.4. Impact Sensitivity Tests. For impact sensitivity tests of raw NQ and ultrafine NQ samples, the drop hammer mass was 10 kg, drop height was 50 cm, and sample mass was 50 ± 1 mg. Each specimen was tested for 25 rounds, and two sets of parallel experiments were done. The result was that the impact sensitivity of both raw NQ and ultrafine NQ samples was 0, and there was no significant difference between the two sets of test results. Therefore, the impact sensitivity of the particles of the ultrafine NQ samples will not increase, and the safety is better.

The lower sensibility of nitroguanidine is related to the stability of its molecular structure.[17,18] The structure of the NQ molecule is shown in Figure 5. The three intermolecular C−N

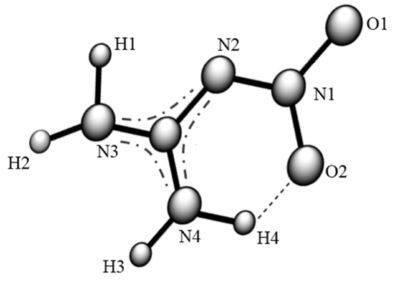

Figure 5. Molecular structure of NQ.

bonds are regionally averaged due to the influence of the off-domain π-electrons between single and double bonds, and the C atoms and the three surrounding N atoms converge to a single plane, increasing the stability of the system.[19] In addition, NQ forms intramolecular and intermolecular hydrogen bonds, and this mesh structure formed by hydrogen bonding is also the most important reason for the stability of this explosive.

3.5. Variation of Bulk Density with Particle Size. The bulk densities of the raw NQ and ultrafine NQ samples were measured by the standard container method, and the results are shown in Table 2. The raw NQ crystals are long needles with a high aspect ratio, and their bulk density is lower. Ultrafine NQ is more densely packed in the same volume due to the smaller

Table 2. Bulk Density of NQ with Different Particle Sizes

sample	shape of particles	aspect ratio	bulk density (g·cm^{-3})
raw NQ	needle-like	8.73	0.36
1#	rectangles	2.26	0.69
2#	rectangles	1.83	0.77
3#	square-like	1.25	0.54

aspect ratio after pulverization, and the corresponding bulk density is higher. However, the particle size of the 3# sample is smaller than that of the 2# sample, but its bulk density is lower, which is due to the increase of cracks on the surface of the sample after the impact of multiple high-speed crushing and shearing, resulting in a decrease in its bulk density. In addition, when the particle size of ultrafine NQ is small to a certain size, the particles are agglomerated due to the large van der Waals forces between the particles, resulting in a decrease in the bulk density of the particles.[20,21] Therefore, in the process of ultrafine NQ, the number of cycle pulverization times should be controlled so that the particle size of ultrafine NQ is within a certain range.

3.6. Thermal Decomposition Property Analysis. The DSC curves of raw NQ and ultrafine NQ samples at different heating rates were measured in an atmospheric pressure N_2 atmosphere, as shown in Figure 6. The decomposition exothermic peak temperature of the ultrafine NQ sample was slightly shifted forward compared with that of the raw material NQ, and the decomposition exothermic peak of NQ gradually decreased with the decrease of particle size. According to the hot spot theory, the thermal decomposition peak temperature of the ultrafine NQ sample was shifted forward due to the decrease of NQ particle size and the increase of specific surface area, which is favorable for heat conduction and makes the hysteresis effect of the measurement result decrease.

Based on the DSC test data, the apparent activation energy of the samples was calculated to assess the decomposition kinetics.[22−25] The apparent activation energy of NQ decomposition was calculated using the Kissinger method and the Starink method.[26,27]

The Kissinger equation describes the linear relationship between $\ln(\beta/T_p^2)$ and $1/T_p$ (Figure 7) as follows

$$\ln\left(\frac{\beta}{T_p^2}\right) = \ln\frac{AR}{E_a} - \frac{E_a}{RT_p} \quad (1)$$

where β is the heating rate, K·min^{-1}; T_p is the peak temperature of decomposition at the corresponding heating rate, K; E_a is the apparent activation energy, kJ·mol^{-1}; A is the apparent pre-exponential factor, min^{-1}; and R is the gas constant, 8.314 J·K^{-1}·mol^{-1}.

In contrast, when the activation energy is calculated by the Starink method, the equation expresses the linear relationship between $\ln(T_p^{1.8}/\beta)$ and $1/T$ (Figure 7) as follows

$$\ln\left(\frac{T_p^{1.8}}{\beta}\right) = \frac{(1.0070 - 1.2\times10^{-5}E_a)E_a}{R\cdot T_p} + \text{const} \quad (2)$$

The calculated results are listed in Table 3. The E_a values calculated using the Kissinger and Starink equations are basically the same, indicating that the calculation of the activation energy is reliable. As can be seen in Figure 3, the activation energies of raw NQ and ultrafine NQ (1#, 2#, and 3#) samples are 144.20, 159.25, 164.48, and 168.47 kJ·mol^{-1}, respectively, which

https://doi.org/10.1021/acsomega.3c06086
ACS Omega 2024, 9, 538−544

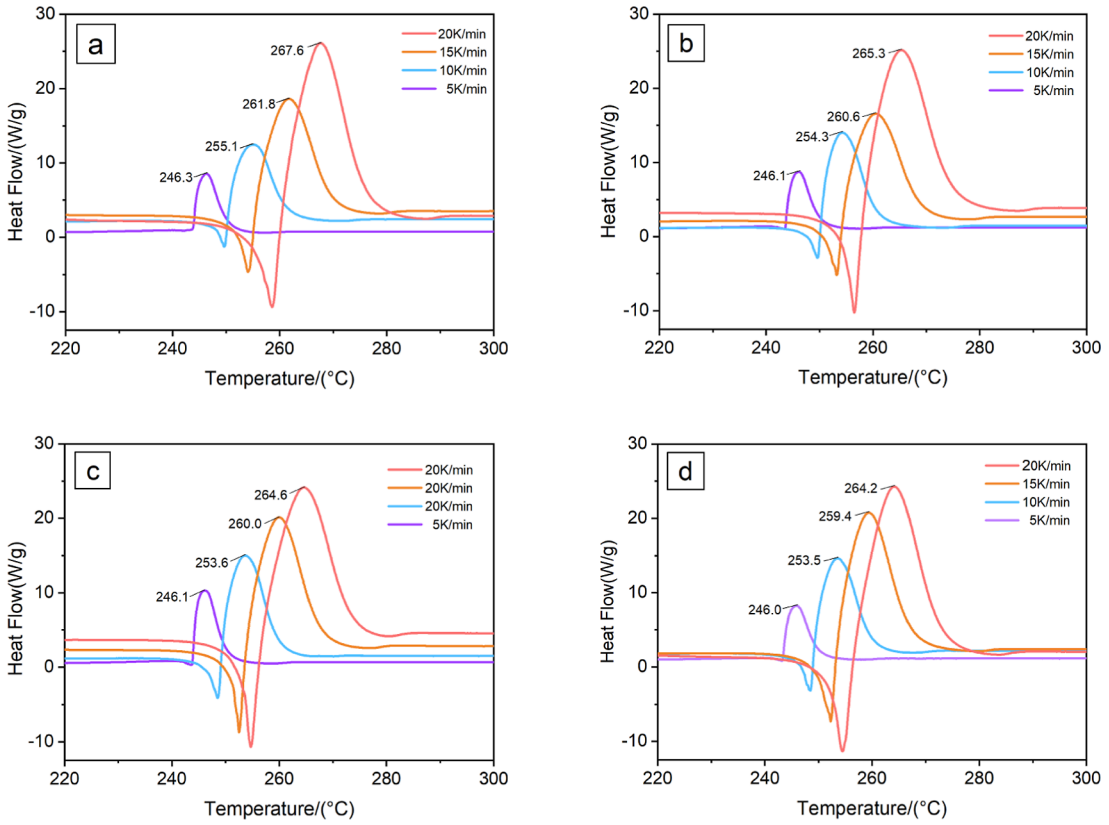

Figure 6. Thermal decomposition curves of raw NQ (a), ultrafine NQ 1# (b), ultrafine NQ 2# (c), and ultrafine NQ 3# (d).

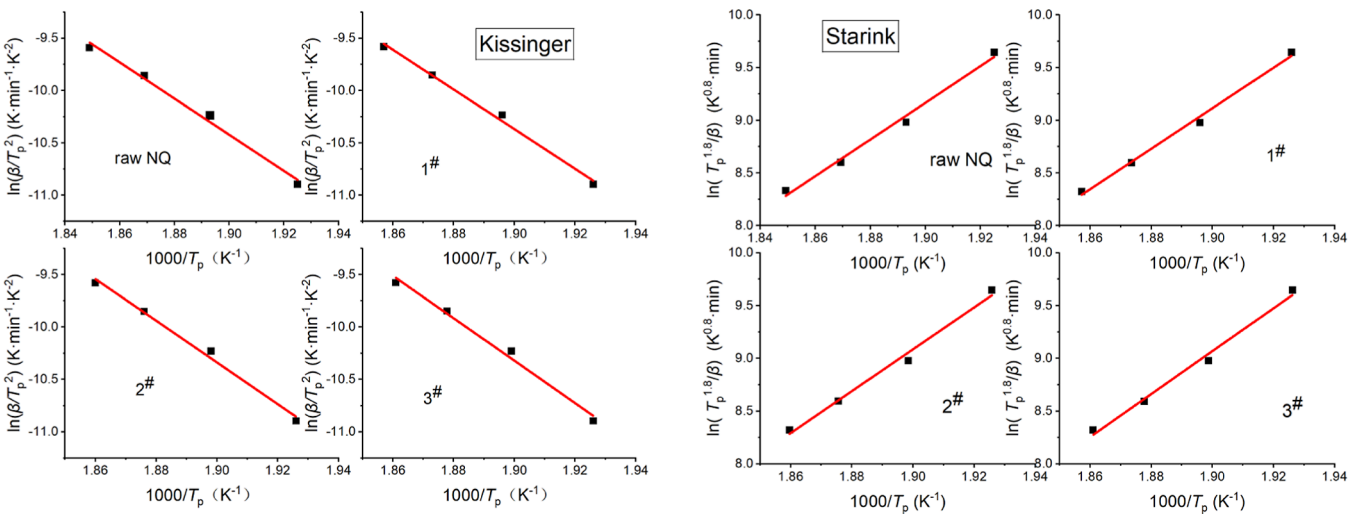

Figure 7. Correlation of apparent activation energy by the Kissinger equation and the Starink equation.

Table 3. Thermal Decomposition Temperatures and Apparent Activation Energies of Raw NQ and Ultrafine NQ Samples

	T_p (°C)					E_a (kJ·mol^{-1})	
sample	5 K/min	10 K/min	15 K/min	20 K/min	Kissinger	Starink	$(E_K + E_S)/2$
raw NQ	246.3	255.1	261.8	267.6	143.75	144.66	144.20
1#	246.1	254.3	260.6	265.3	158.80	159.70	159.25
2#	246.1	253.6	260.0	264.6	164.04	164.93	164.48
3#	246.0	253.5	259.4	264.2	168.03	168.90	168.47

indicates that the smaller the particle aspect ratio of the NQ crystals, the higher the energy required to reach the activation state. This is due to the fact that the particle size of the ultrafine NQ particles decreases, the internal defects of the particles are modified, and when subjected to heat, the stress concentration

https://doi.org/10.1021/acsomega.3c06086
ACS Omega 2024, 9, 538−544

suffered is improved, and the crystals become more difficult to destroy, so their thermal stability becomes better.

Based on the calculation of the apparent activation energy, other thermal property data such as entropy, enthalpy, and Gibbs free energy were obtained using the equations. The eqs 3−5 were calculated as follows

$$\Delta G = RT\ln\left(\frac{k_B R}{h}\right) + E_a \quad (3)$$

$$\Delta H = E_a - RT \quad (4)$$

$$\Delta G = \Delta H - T\Delta S \quad (5)$$

where ΔH is the enthalpy change, kJ·mol^{-1}; ΔS is the entropy change, J·mol^{-1}·K^{-1}; ΔG is the Gibbs free energy change, kJ·mol^{-1}; k_B is Boltzmann's constant, J·K^{-1}; and h is Planck's constant, J·s^{-1}. Calculations are given in Table 4.

Table 4. Thermal Performance Data Related to Raw NQ and Ultrafine NQ

sample	ΔH (kJ·mol^{-1})	ΔS (J·mol^{-1}·K^{-1})	ΔG (kJ·mol^{-1})
raw NQ	140.03	−258.45	276.56
1#	154.71	−258.44	291.02
2#	159.82	−258.43	295.94
3#	163.70	−258.42	299.80

The ΔS and ΔG of the activation process of raw NQ and ultrafine NQ samples are almost the same and greater than zero, which indicates that the thermal decomposition process of NQ is nonspontaneous and needs to absorb heat from the outside world, and ΔH represents the heat energy absorbed by the NQ molecules when they are transformed into activated molecules. The ΔH and ΔG of the thermal decomposition of the ultrafine NQ samples are smaller than those of the raw NQ, which indicates that the raw NQ needs to obtain more heat than the ultrafine NQ when thermal decomposition of the NQ crystals occurs, which further indicates that the thermal stability of the ultrafine NQ is better.

4. CONCLUSIONS

Ultrafine NQ was prepared by the mechanical pulverization method and the spray drying method, the D_{50} of the resulting samples could reach less than 10 μm, the particle size distribution was concentrated, no impurities were introduced during the refinement process, and the samples were of high purity. Compared with the raw NQ, the impact sensitivity of the ultrafine NQ samples did not change significantly, the crystal defects were reduced, the bulk density first became higher with the reduction of the particle size, and when the particle size was small to a certain size, the bulk density was reduced instead, so the prepared ultrafine NQ should be controlled within a certain particle size range. In addition, the thermal stability of NQ samples becomes better with a decrease of the particle aspect ratio.

AUTHOR INFORMATION

Corresponding Author

Xiaoan Wei − *School of Chemical Engineering, Nanjing University of Science and Technology, Nanjing 210094, China*; Email: weixiaoan@126.com

Authors

Dan Liang − *School of Chemical Engineering, Nanjing University of Science and Technology, Nanjing 210094, China*; orcid.org/0009-0008-8581-2169

Wenjing Zhang − *School of Chemical Engineering, Nanjing University of Science and Technology, Nanjing 210094, China*

Sheng Wang − *School of Chemical Engineering, Nanjing University of Science and Technology, Nanjing 210094, China*

Binbin Wang − *School of Chemical Engineering, Nanjing University of Science and Technology, Nanjing 210094, China*

Zeshan Wang − *School of Chemical Engineering, Nanjing University of Science and Technology, Nanjing 210094, China*

Complete contact information is available at: https://pubs.acs.org/10.1021/acsomega.3c06086

Notes

The authors declare no competing financial interest.

ACKNOWLEDGMENTS

The authors would like to thank the Key Laboratory of Specialty Energy Materials, Ministry of Education, Nanjing, for supporting this work.

REFERENCES

(1) Samudre, S. S.; Nair, U. R.; Gore, G. M.; Kumar Sinha, R.; Kanti Sikder, A.; Nandan Asthana, S. Studies on an improved plastic bonded explosive (PBX) for shaped charges. *J. Propell. Explos. Pyrot.* **2009**, *34*, 145−150.

(2) Altenburg, T.; Klapötke, T.; Penger, A.; Stierstorfer, J. Two outstanding explosives based on 1,2-dinitroguanidine: ammonium-dinitroguanidine and 1,7-diamino-1,7-dinitrimino-2,4,6-trinitro-2,4,6-triazahept-ane. *J. Z. Anorg. Allg. Chem.* **2010**, *636*, 463−471.

(3) Wang, B.; Liao, X.; Wang, Z.; DeLuca, L. T.; Liu, Z.; He, W. Effects of particle size and morphology of NQ on thermal and combustion properties of triple-base propellants. *J. Combust. Flame* **2018**, *193*, 123−132.

(4) Pritchard, E. J.; Wright, G. F. Production of nitroguanidine with high bulk-density. *Can. J. Res., Sect. F* **1947**, *25f*, 257−263.

(5) Luo, Z.; Cui, Y.; Dong, W.; Xu, Q.; Zou, G.; Kang, C.; Hou, B.; Chen, S.; Gong, J. Morphological diversity of nitroguanidine crystals with enhanced mechanical performance and thermodynamic stability. *J. Cryst. Growth* **2017**, *480*, 132−140.

(6) Tisdale, J. T.; Hill, L. G.; Duque, A. L. Production of desensitized, ultrafine PETN powder. *J. Powder Technol.* **2022**, *396*, 152−157.

(7) Hu, L.; Chen, M. Preparation of ultrafine powder: the frontiers of chemical engineering. *J. Mater. Chem. Phys.* **1996**, *43*, 212−219.

(8) Pant, A.; Nandi, A. K.; Newale, S. P.; Gajbhiye, V. P.; Prasanth, H.; Pandey, R. K. Preparation and characterization of ultrafine RDX. *Cent. Eur. J. Energy Mater.* **2013**, *103*, 393−407.

(9) Li, J. S.; Wu, S. W.; Lu, K. T. Study on preparation of insensitive and spherical high bulk density nitroguanidine with controllable particle size. *J. Propell. Explos. Pyrot.* **2016**, *41*, 312−320.

(10) Li, H.; Ren, H.; An, Y.; Liu, Y.; Yuan, Z. Preparation of ultrafine nitroguanidine by one-step crystallization in an impinging stream-rotating packed bed. *J. Ind. Eng. Chem. Res.* **2023**, *62*, 5141−5149.

(11) Yang, J.; Cui, Y.; Chen, M.; Wang, Y.; Xu, S.; Wu, S.; Wang, J.; Gong, J. Transformation between two types of spherulitic growth: tuning the morphology of spherulitic nitroguanidine in a gelatin solution. *J. Ind. Eng. Chem. Res.* **2020**, *59*, 21167−21176.

(12) Teipel, U. Production of particles of explosives. *J. Propell. Explos. Pyrot.* **1999**, *24*, 134−139.

(13) Retsch Technology. Optimising the measurement of fine particles. *Metal Powder Report*; Elseiver, 2013; Vol. 68, pp 34−37.

(14) *GJB 772A. Explosive Test Method*; China Weapons Industry Press: Bejing, 1997.

(15) Inaba, K.; Matsumoto, K. The development of the measurement of particle concentration using a commercial laser diffraction particle size analyzer. *J. Adv. Powder Technol.* **1999**, *10*, 89−103.
(16) Murmann, R. K.; Glaser, R.; Barnes, C. L. Structures of nitroso- and nitroguanidine X-ray crystallography and computational analysis. *J. Chem. Crystallogr.* **2005**, *35*, 317−325.
(17) Bracuti, A. J. Crystal structure refinement of nitroguanidine. *J. Chem. Crystallogr.* **1999**, *29*, 671−676.
(18) Bryden, J. H.; Burkardt, L. A.; Hughes, E. W.; Donohue, J. The Crystal Structure of nitroguanidine. *J. Acta. Cryst.* **1956**, *9*, 573−578.
(19) Dan, Z.; Guo, X.; Lin, H.; Ou, Y.; Dong, B.; Wang, G. Preparation and performance research of ultra-fine nitroguanidine. *J. Solid Rocket Technol.* **2015**, *38*, 847−852.
(20) Li, Q.; Rudolph, V.; Peukert, W. London-van der Waals adhesiveness of rough particles. *J. Powder Technol.* **2006**, *161*, 248−255.
(21) Hamaker, H. C. The London-van der Waals attraction between spherical particles. *Physica* **1937**, *4*, 1058−1072.
(22) Liu, Z. T.; Zhang, F.; Du, P.; Xu, B. Effect of NQ content on the thermal decomposition of nitroguanidine propellant using isoconversional methods. *J. Therm. Anal. Calorim.* **2019**, *137*, 473−480.
(23) Vyazovkin, S.; Burnham, A. K.; Criado, J. M.; Pérez-Maqueda, L. A.; Popescu, C.; Sbirrazzuoli, N. ICTAC Kinetics Committee recommendations for performing kinetic computations on thermal analysis data. *J. Thermochim. Acta* **2011**, *520*, 1−19.
(24) Zhang, F.; Liu, Z. T.; Du, P. Thermal decomposition kinetics of nitroguanidine propellant under different pressures. *J. Propell. Explos. Pyrot.* **2018**, *43*, 390−397.
(25) Gao, W.; Liu, X.; Su, Z.; Zhang, S.; Yang, Q.; Wei, Q.; Chen, S.; Xie, G.; Yang, X.; Gao, S. High-energy-density materials with remarkable thermostability and insensitivity: syntheses, structures and physicochemical properties of Pb(II) compounds with 3-(tetrazol-5-yl) triazole. *J. Mater. Chem. A* **2014**, *2*, 11958−11965.
(26) Kissinger, H. E. Reaction kinetics in differential thermal analysis. *Anal. Chem.* **1957**, *29*, 1702−1706.
(27) Starink, M. J. A new method for the derivation of activation energies from experiments performed at constant heating rate. *J. Thermochim. Acta* **1996**, *288*, 97−104.

https://doi.org/10.1021/acsomega.3c06086
ACS Omega 2024, 9, 538−544